Confinement Experiments of Pure Ion and Electron Plasmas in a Nested Trap*)

Toshikazu OKADA, Haruhiko HIMURA, Yutaro NAKAJIMA and Akio SANPEI

Department of Electronics, Kyoto Institute of Technology, Kyoto 606-8585, Japan

(Received 9 January 2023 / Accepted 26 June 2023)

We perform experiments where lithium ion and electron plasmas are simultaneously confined in a nested trap to detect two-fluid plasma states. However, the behavior of charged particles in the nested trap is unexplained. Results of experiments demonstrate that the number of charged particles in the outer wells of the nested trap rapidly decreases and that peculiar deformations in ion and electron plasmas cause in some conditions.

Keywords: non-neutral plasma, nested trap, confinement

DOI: 10.1585/pfr.18.2401072

1. Introduction

The two-fluid plasma model [1] is a fluid model that uses different equations of motion to describe the motions of electron and ion fluids. Thus, this model allows independent fluid motions of them with corresponding velocity fields. This model is employed to explain some phenomena, including high-β equilibrium [2] and peripheral plasmas surrounding their high-temperature core [3]. When the ratio of the characteristic scale length of the plasma L to the ion skin depth $\lambda_i = c/\omega_{pi}$ is less than ~ 30, such independent motions are predicted to considerably appear [4, 5]. The plasmas that are created in a laboratory are usually not in this regime; hence, no clear-cut experiment on two-fluid plasmas has been reported. Additionally, the two-fluid plasma model applies to electrically non-neutral plasmas [6] because ion density n_i and electron density n_e appear explicitly in these equations. Then, to observe two-fluid plasma states experimentally, we superimpose pure ion plasma over pure electron plasma in the BX-U [7].

We use a nested trap for superimposition experiments. The nested trap is a charged-particle trap with nested positive and negative potential wells [8], which makes it possible to confine positive ions and electrons in the same region simultaneously. However, it is unclear how long non-neutral plasmas can be confined and how they behave in the nested trap. In this study, we present the results of superimposition experiments to confine non-neutral plasmas in the nested trap.

2. Setup

Figure 1 (a) shows a schematic of the BX-U [7]. The typical pressure of a central vacuum vessel is $\approx 4 \times 10^{-9}$ Torr. A uniform magnetic field of 0.12 T is applied to the entire vacuum vessel using solenoid coils in the right direction in Fig. 1 (a). The BX-U comprises a set of 23 electrically isolated cylindrical electrodes (we refer to them as multi-ring electrodes) in this vacuum vessel. The multi-ring electrodes have inner diameter of 100 mm and a total length of 782 mm. By applying an external voltage to each electrode individually, potential profiles, as shown in

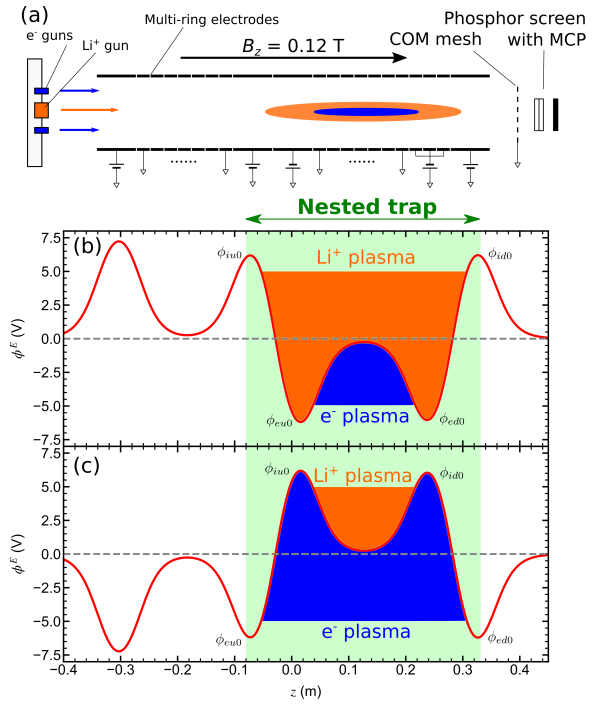

Fig. 1 (a) Schematic of BX-U. The BX-U machine comprises a gun holder with electron guns and an ion gun, multi-ring electrodes, and a phosphor screen with microchannel plate. (b) One of the potential profiles of the nested traps at $r = 0$. In this nested trap, a negative potential well is formed inside a positive potential well. (c) The other type of nested traps. In this nested trap, a positive potential well is formed inside a negative potential well.

author's e-mail: d1822001@edu.kit.ac.jp

*) This article is based on the presentation at the 31st International Toki Conference on Plasma and Fusion Research (ITC31).

Figs. 1 (b) and (c) in solid curves, can be formed inside them. The regions with a background (green in color) in both Figs. 1 (b) and (c) are the nested trap. Figure 1 (b) shows the formation of a negative potential well inside a positive potential well. Conversely, Fig. 1 (c) shows the formation of a positive potential well inside a negative potential well. The nested traps can be formed by controlling the external voltage applied to the multi-ring electrodes.

The orange- and blue-colored squares on the left side of Fig. 1 (a) represent the placement of one Li^+ gun and four e^- guns upstream of the BX-U, respectively. The e^- guns are placed at a distance of 26±2 mm from the machine axis. The electron sources are heated using a heater at ~ 1000°C. Electric fields are used to extract thermal electrons from cathodes and extractors. The initial energy of e^- beam is determined by the acceleration voltage V_{eA} applied to the cathode. The Li^+ gun is placed on the machine axis. The Li^+ beam is extracted by heating the β-eucryptite to ~ 1000°C using a heater and applying a voltage to an anode and an extractor. The initial energy of the ions is determined using the acceleration voltage V_{iA} applied to the anode.

For the measurement, a microchannel plate (MCP) is placed at $z = 0.6$ m [9]. The effective diameter of the MCP is 40 mm. Ions and electrons, confined in the trap, flow out toward the MCP as the potential barrier ϕ_{id0} or ϕ_{ed0} on the right side of Figs. 1 (b) or (c) reduces to 0 V. Numerous secondary electrons are ejected from the MCP when charged particles collide with the MCP. These secondary electrons are further accelerated by applying a voltage of approximately 3 kV and hit a phosphor screen. The fluorescence of the phosphor screen is captured using a camera. The resulting images correspond to the line-integrated density distribution of Li^+ or e^- plasmas.

3. Experimental Results

First, Li^+ and e^- plasmas are superimposed in the nested trap as shown in Fig. 1 (b). This experiment is denoted as Expt. 1. In Expt. 1, the ion density n_i is 1.2×10^{10} m^{-3} and the electron density n_e is 6.0×10^{12} m^{-3}. The fractional charge neutralization f in this experiment is 0.002, where fractional charge neutralization f is defined as $f = n_i/n_e$ [10]. To prevent generation of impurity ions, potential barriers are set to $\phi_{iu0}, \phi_{id0} = 10$ V and $\phi_{eu0}, \phi_{ed0} = -10$ V [11]. It should be noted that the ion skin depth λ_i in the experiment is 5.1×10^3 m, which is relatively longer than plasma radii (~ 1 cm) confined in the BX-U. Thus, λ_i/L is relatively larger than ~ 1/30. Furthermore, the series of experimental data is obtained shot-by-shot.

Figure 2 shows the images of the luminescence of the phosphor screen obtained in Expt. 1. These image data are captured in the same method as in references [12–14]. Here, the vertical shadow in the image is the shadow of a wire [15] that is installed inside the vessel when this series of experiments is performed. The wire is installed to measure the azimuthal rotation velocity $v_{\sigma\theta}$ of the Li^+ or e^- plasma. However, this shadow is disregarded in this series of experiments.

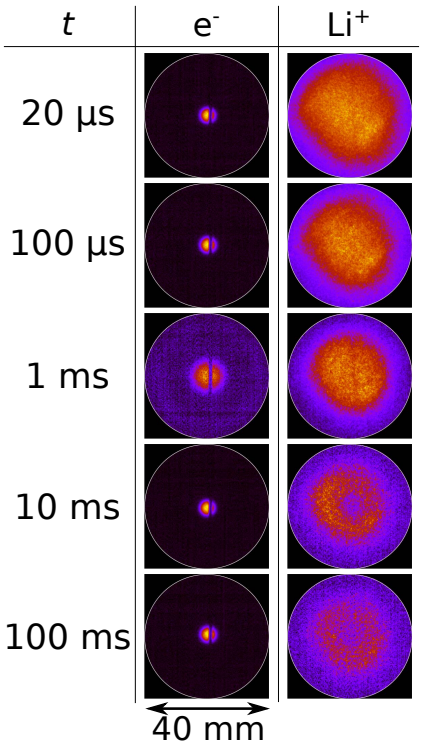

Fig. 2 Images obtained in Expt. 1. Images in the left row and right row are obtained when e^- plasmas and Li^+ plasmas are ejected from the nested trap, respectively. The white circles drawn in all images show the effective surface of the MCP with a diameter of 40 mm. These experiments are performed in the nested trap as shown in Fig. 1 (b).

The e^- plasma is located at the center of the images and does not deform until the superposition time $t = 100$ μs and Then, the e^- plasma appears to be expanding at 1 ms. After that, the center of the phosphor screen is emitted with approximately the same radius as $t \leq 100$ μs until 100 ms. Furthermore, the Li^+ plasma appears elliptically deformed at $t = 20$ μs. Thereafter, the luminosity and plasma radius gradually decrease until 1 ms. The Li^+ plasma deforms into a hollow-like shape at 10 ms and maintains that shape until 100 ms.

Next, Fig. 3 indicates the image data obtained by superimposing Li^+ and e^- plasma in the nested trap shown in Fig. 1 (c). Figure 3 (a) shows the results when $n_i = 1.8 \times 10^{10}$ m^{-3}, $n_e = 1.2 \times 10^{11}$ m^{-3}, i.e., $f = 0.15$ (Expt. 2). Whereas, Fig. 3 (b) shows the results when $n_i = 1.8 \times 10^{10}$ m^{-3}, $n_e = 2.4 \times 10^{10}$ m^{-3}, i.e., $f = 0.74$ (Expt. 3). For both experiments, potential barriers are $\phi_{iu0}, \phi_{id0} = 10$ V and $\phi_{eu0}, \phi_{ed0} = -10$ V. It should be noted that the λ_i is 4.1×10^3 m in both experiments, which is adequately long.

In Expt. 2, the e^- plasma expands from $t = 20$ μs to 5 ms, despite remaining at the center. The e^- plasma shifts ~ 15 mm from the center of the image after 10 ms. The Li^+ plasma looks elliptically deformed at $t = 20$ μs, as

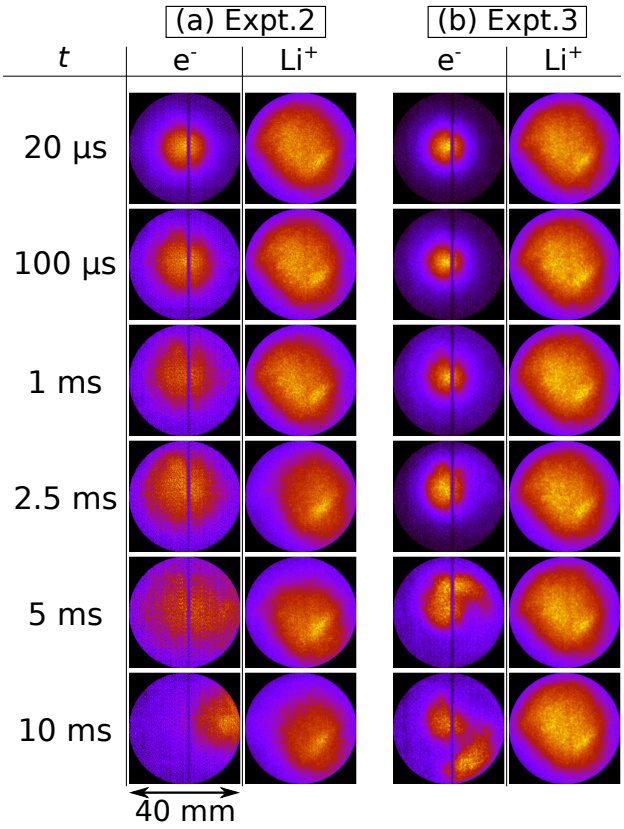

Fig. 3 Images obtained in Expts. 2 and 3. These experiments are performed in the nested trap shown in Fig. 1 (c).

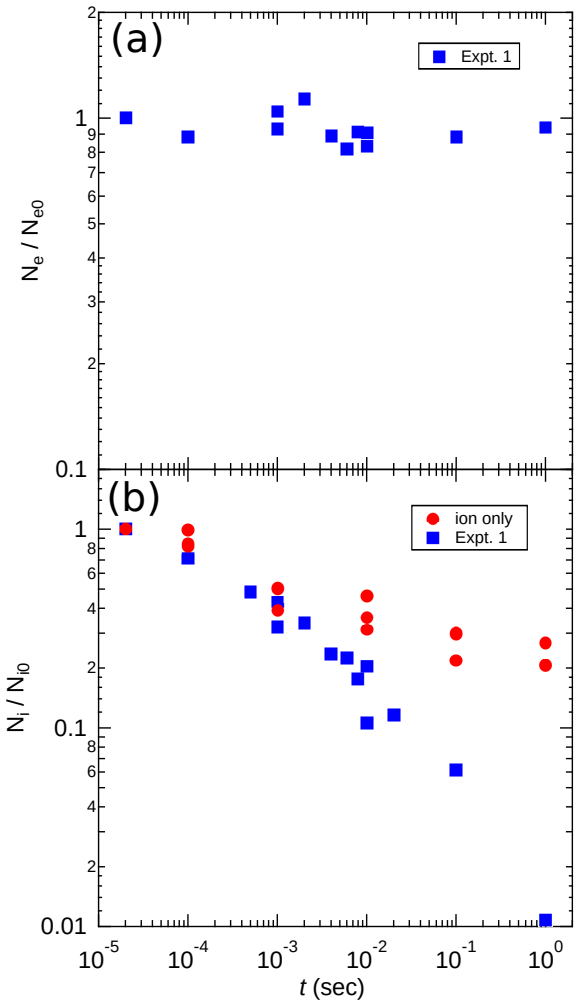

Fig. 4 Dependence of the number of (a) electrons and (b) ions on confinement time in Expt. 1. Figure (b) also shows the confinement time dependence of the number of ions when only ions are confined in the nested trap (colored in red).

in Expt. 1. Then, the Li^+ plasma maintains its shape until 1 ms. The Li^+ plasma shifts to the lower right of the image at 2.5 ms and never come to the center of the image until 10 ms. At Expt. 3, e^- plasma shows no deformation in $t \leq$ 1 ms. The e^- plasma shifts slightly off-center at 2.5 ms and deforms into a tail-like at 5 ms. Then, the e^- plasma splits into two populations at 10 ms, one near the center and the other extending tail-like at about 15 mm away from the center. Despite significant deformation in the e^- plasma, the Li^+ plasma maintains its shape at $t = 20$ μs until 10 ms later.

Figures 2 and 3 show the number of Li^+ and e^- particles are related to the total luminescence of the images [9]. Charged particles flowing out of the nested trap pass through a COM mesh that is grounded. The COM mesh is attached to the incident side of the MCP with an open area ratio β. Then charged particles collide with the MCP. The effective gain of the MCP, i.e., the ratio of the number of secondary electrons to the number of charged particles colliding with the MCP, αG is experimentally defined as $\alpha G = C_\sigma \times (\Delta U_M)^{20.2}$, where C_σ and ΔU_M represent a factor and a voltage applied to MCP, respectively. The value of C_σ is known to be ~ 337 for Li^+ and ~ 196 for e^-. Additionally, the ratio ξ of the total amount of luminosity of the phosphor screen to the number of secondary electrons was discovered to be $\approx 1 \times 10^{-5}$. Thus, there is a relationship of $N_\sigma = L/\xi\beta\alpha G$ between the total luminosity L and the number of charged particles N_σ.

Figure 4 shows the calculated number of charged particles that reach the MCP in Expt. 1. Figure 4 (a) shows the dependence of the number of electrons flowing out when ϕ_{ed} is reduced to 0 V on the superposition time t. Here, N_{e0} is the number of electrons at $t = 20$ μs, $N_{e0} \approx 10^8$. It is discovered that, despite a variance of ±15%, the number of electrons is almost constant for ~ 1 s. Figure 4 (b) shows the dependence of the number of ions on confinement time. Here, N_{i0} is the number of ions at $t = 20$ μs, $N_{i0} \approx 10^5$. The plot points in blue and red represent the results when the Li^+ plasma is superimposed on the e^- plasma and when only the Li^+ plasma is confined in the nested trap, respectively. When only Li^+ plasma is confined, the ion number decreases to ~ 20% of N_{i0} after 1 s. In contrast, when superimposed with e^- plasma, the number of ions drops to about 1% after 1 s. The decrease in the number of ions corresponds to the decrease in the total luminosity of the images. Additionally, there is no substantial difference in

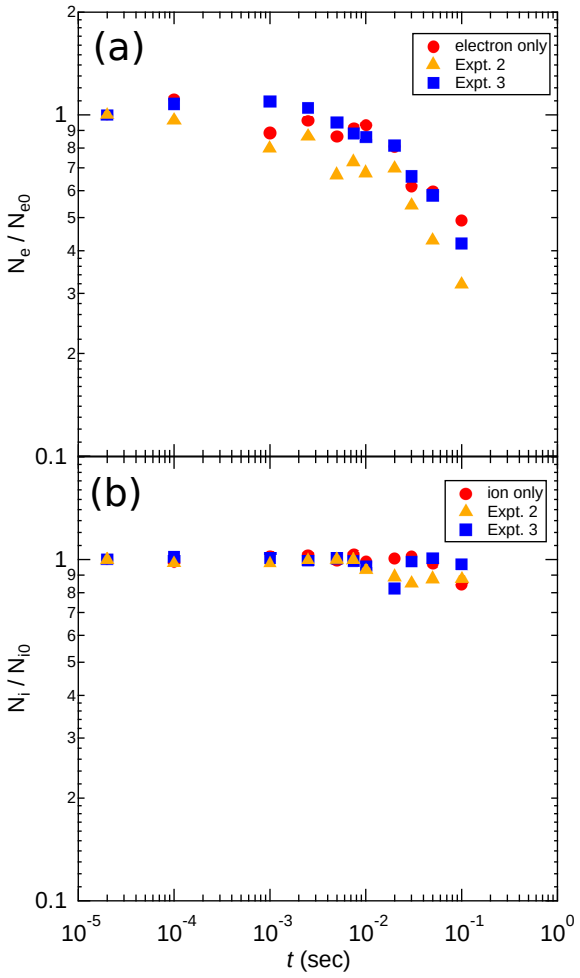

Fig. 5 Dependence of the number of (a) electrons and (b) ions on confinement time in Expts. 2, 3, which are colored yellow and blue, respectively. Figures (a) and (b) show the confinement time dependence of the number of electrons/ions when only electrons/ions are confined in the nested trap and are also plotted in red.

the rate of decrease between the case with and without e^- plasma superimposed until ~ 1 ms. However, for $t \geq 1$ ms, the number of ions decreases more rapidly when superimposed than when only Li^+ plasma is confined in the nested trap.

Figure 5 (a) shows the dependence of the number of electrons on confinement time for Expts. 2, 3 and when only e^- plasma is confined in the nested trap, where $N_e 0 \approx 10^6, 10^5$ and 10^6, respectively. When only electrons are confined in the nested trap, more than 90% of the number of electrons is maintained for ~ 10 ms. Thereafter, the electron number gradually drops to about 50% at 100 ms. The number of electrons in Expt. 2 drops to about 70% in ~ 1 ms. Thereafter, it maintains a lower fraction than when only electrons are confined. This corresponds to the electrons expanding and diffusing outward from the effective area of the MCP (see Fig. 3 (a)). The number of electrons in Expt. 3 decreases similarly to when only electrons are confined. Figure 5 (b) shows the dependence of the number of ions on confinement time for Expts. 2, 3 and when only Li^+ plasma is confined in the nested trap, with $N_{i0} \approx 10^5$ in each case. In all cases, the number of ions keeps approximately 100% for ~ 10 ms. Then, at Expt. 2, it drops to about 85%, corresponding to the deformation of the Li^+ plasma shape and some ions moving out of the effective area of the MCP (see Fig. 3 (b)).

4. Discussion & Conclusion

Figures 4 and 5 show the dependence of the number of ions and electrons on the confinement time in the nested traps. According to Figs. 4 (a) and 5 (b), the confinement time of charged particles trapped in the inner well of the nested trap is longer than 1 s. Since the geometry of the inner well is substantially identical to that of the Penning-Malmberg trap, it is expected that confinement property is equivalent to that of the Penning-Malmberg trap. However, from Figs. 4 (b) and 5 (a), the confinement time of charged particles trapped in the outer well of the nested trap is shorter than 1 s. Charged particles are not thermalized in the outer well of the nested trap. Even high-energy electrons are produced, which generate impurity ions [11]. These phenomena should be related to the short-time confinement of charged particles in the pair of outer wells of the nested trap. However, as shown in Fig. 5, there is a condition where the number of both Li^+ and e^- does not drop for about 10 ms in the nested trap shown in Fig. 1 (c). In the BX-U, the collision time between electrons and neutrals is $\approx$ 0.3 s. Thus, although electrons are also accelerated by the external electric field that forms the nested trap, the number of electrons does not drop for about 10 ms since electrons rarely collide with neutrals.

Furthermore, some peculiar phenomena are observed in the superposition experiments in the nested trap. Figure 2 shows the result of the hollow distribution of Li^+ plasmas. Moreover, Fig. 3 shows the expansion and large deformation of e^- plasmas. These phenomena are observed only when electrons and ions are confined simultaneously in the nested trap. One may consider that the observed deformation is caused due to ion resonance instability [16]. However, the deformation is never growing but saturated. The large value of λ_i / L may be related to this non-linear saturation.

[1] B. Srinivasan and U. Shumlak, Phys. Plasmas **18** (9), 092113 (2011).
[2] D.C. Barnes, Phys. Plasmas **10**, 1636 (2003).
[3] B. Zhu *et al.*, Comput. Phys. Commun. **232**, 46 (2018).
[4] H. Himura, IEEJ Trans. Fundam. Mater. **130** (10), 977 (2010).
[5] S. Kawai *et al.*, Phys. Plasmas **23** (2), 022113 (1995).
[6] Y. Nakajima *et al.*, J. Plasma Phys. **87** (4), 905870415 (2021).
[7] H. Himura, Nucl. Instrum. Methods Phys. Res. B **811**, 100 (2016).
[8] J.R. Danielson *et al.*, Rev. Mod. Phys. **87** (1), 247 (2015).

[9] H. Himura, S. Nakata and A. Sanpei, Rev. Sci. Instrum. **87** (6), 063306 (2016).
[10] R.C. Davidson, *Physics of nonneutral plasmas* (World Scientific Publishing Company, 2001).
[11] T. Okada, H. Himura, S. Yamada, S. Nishio and A. Sanpei, Phys. Lett. A **460**, 128617 (2023).
[12] H. Himura *et al.*, Plasma Fusion Res. **12**, 1201037 (2017).
[13] H. Himura *et al.*, AIP Conf. Proc. **1928**, 020005 (2018).
[14] S. Yamada *et al.*, AIP Conf. Proc. **1928**, 020016 (2018).
[15] Y. Nakajima, H. Himura and T. Okada, AIP Advances **12** (4), 045015 (2022).
[16] G. Bettega *et al.*, Phys. Plasmas **13** (11), 112102 (2006).